Distinguishing Engineered TiO_2 Nanomaterials from Natural Ti Nanomaterials in soil using spICP-TOFMS and Machine Learning

- Supplemental Information

Garret D. Bland[†, §], Matthew Battifarano[†], Ana Elena Pradas del Real[‡], Géraldine Sarret[‡], and Gregory V. Lowry[†, §, *]

[†]Department of Civil and Environmental Engineering, Carnegie Mellon University, Pittsburgh, Pennsylvania 15213, United States

[‡]ISTerre (Institut des Sciences de la Terre), Univ. Grenoble Alpes, CNRS, 38000, Grenoble, France

[§]Center for Environmental Implications of NanoTechnology (CEINT), Carnegie Mellon University, Pittsburgh, Pennsylvania 15213, United States

Number of pages: 31

Number of figures: 22

Number of tables: 5

Summary of Support Information

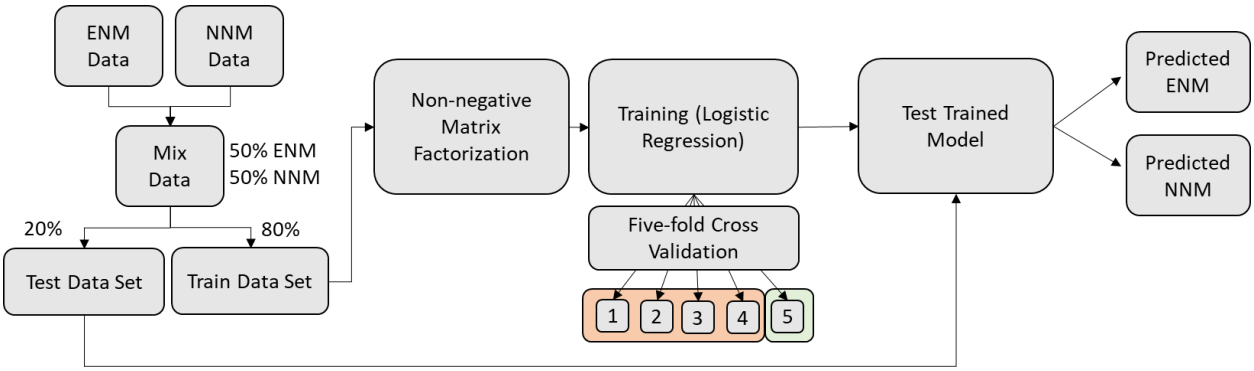

Figure S1: Machine Learning Schematic for classifying ENMs and NNMs

NP Characterization

Table S1: Size distribution of Ti30 and Ti100 samples by DLS, TEM, and spICP-TOFMS. Units are nm.

Sample ID	DLS (Intensity)	DLS (Number)	TEM	ICP-TOFMS*
Ti30	141 ± 31	89 ± 7	31 ± 8	50 ± 21
Ti100	167 ± 27	126 ± 5	125 ± 44	161 ± 60

* spICP-TOFMS measures Ti mass. To calculate size, we assume a spherical shape, anatase density for Ti30 (3.78 g cm^{-3}), and rutile density for Ti100 (4.23 g cm^{-3}).

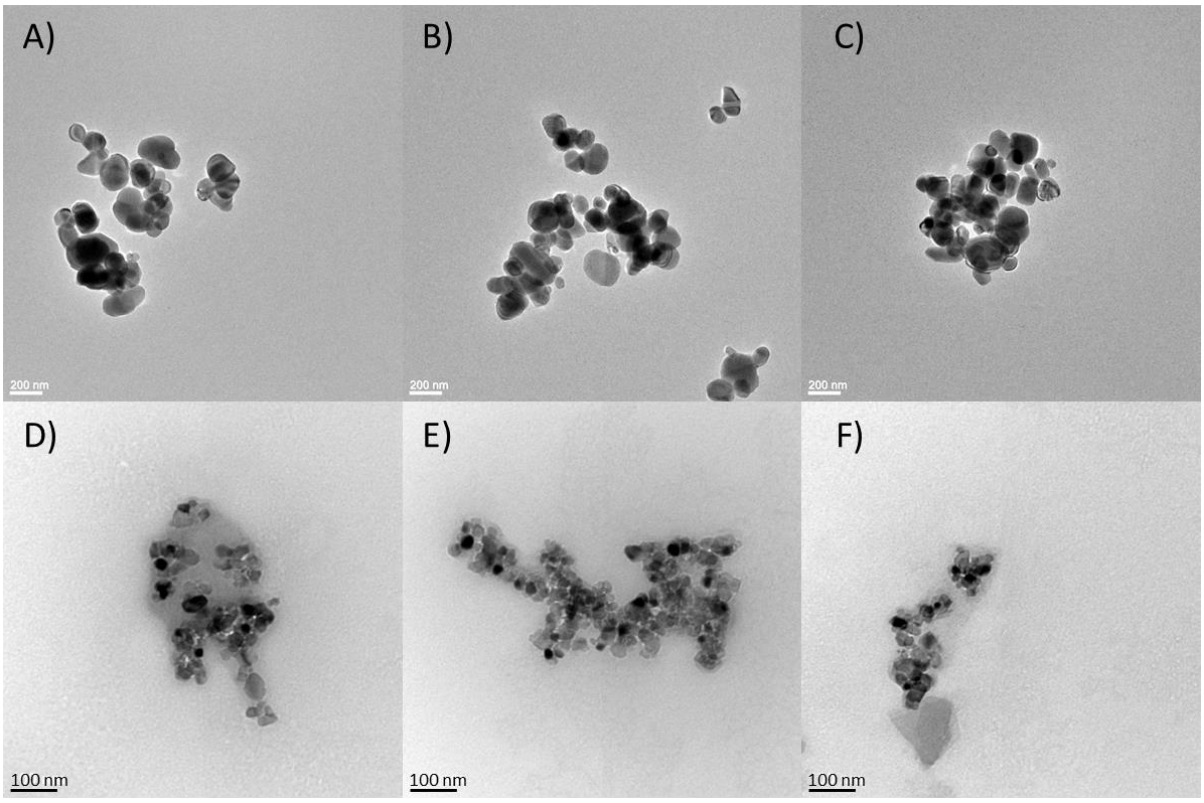

Figure S2: TEM images for Ti100 (A, B, and C) and Ti30 (D, E, and F).

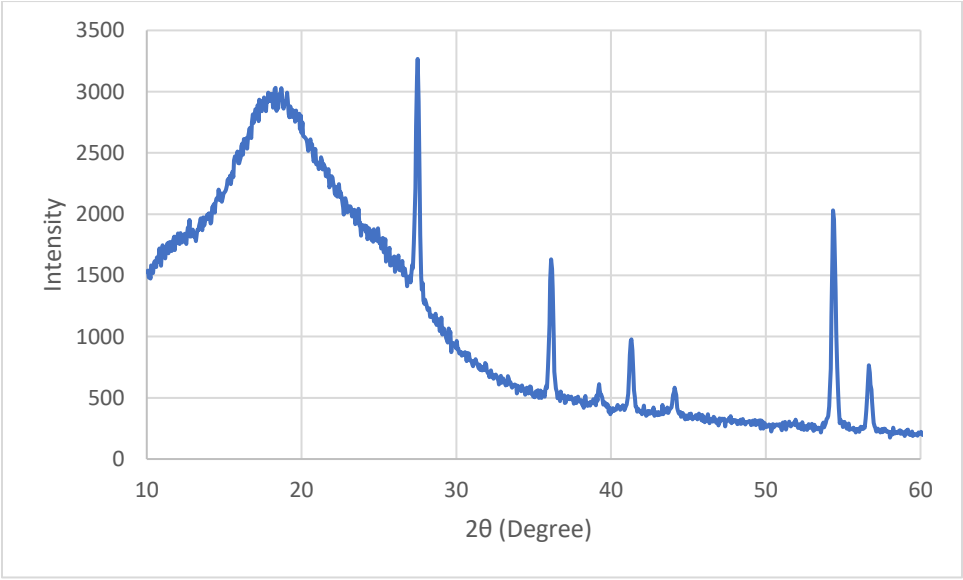

Figure S3: Ti100 XRD Spectrum. All major peaks identify as the rutile form of TiO_2 (27, 36, and 55 degrees).

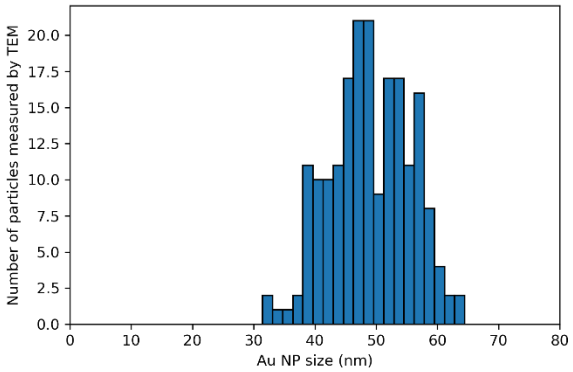

Figure S4: TEM size distribution of the 50 nm reference Au NP used for analysis. Average is 49.1 nm, median is 48.6 nm, and the standard deviation is 6.5 nm. Number of particles equal 193.

Soil Characterization and Experimental Design table

The table below show experimental design matrix to assess classification between ENMs and NNNMs. This table also describes organic carbon (OC) content, pH, and soil type for each soil. L22 soil and AZ soil pH was measured by 1:2 soil to 0.01 M $CaCl_2$ solution ratio. LUV soil was measured by 1:5 ratio. Soil properties were described and measured elsewhere.[1–3]

Table S2: Experimental design matrix for this study. Further soil and sludge characterization is described elsewhere.[2,3]

		Engineered or Recovered Nanomaterials		
	Materials tested	Ti30 TiO_2 particles Size = 30nm	Ti100 TiO_2 particles Size = 100nm	Recovered Ti-NMs Ti-particles recovered from Sludge
Natural Nanomaterials	Lufa 2.2 Soil OC content = 1.71% pH = 5.8 Classification = Loamy Sand	Figure 3B	Figure 3A	Figure 3C
	Luvisol Soil OC content = 2.23% pH = 6.4 Classification = Loam Soil	Figure S10A	Figure 11A	Figure S10C
	Arizona Soil OC content = 0.54% pH = 7.6 Classification = Clayey Loam	Figure S10B	Figure 11B	Figure S10D

Other Machine Learning Models

Table S3: The classification performance results of each ML model for the Ti100 + L22 Case. (>75% = correct, 25% to 75% = uncertain, <25% = incorrect). Number of simulations = 9. Average percentage values are reported with standard deviation in parentheses.

Model Type	*Certain (> 75%)*	*Uncertain (25% to 75%)*	*Incorrect (< 25%)*
RFC	**84.5** (2.0)	**8.7** (1.2)	**6.8** (1.3)
GBC	**85.7** (1.0)	**8.9** (1.0)	**5.3** (0.4)
NN1	**87.1** (0.4)	**6.8** (0.5)	**6.1** (0.6)
NN2	**78.0** (1.3)	**17.2** (0.9)	**4.7** (0.6)
LR	**80.3** (1.3)	**15.2** (1.2)	**4.5** (0.5)

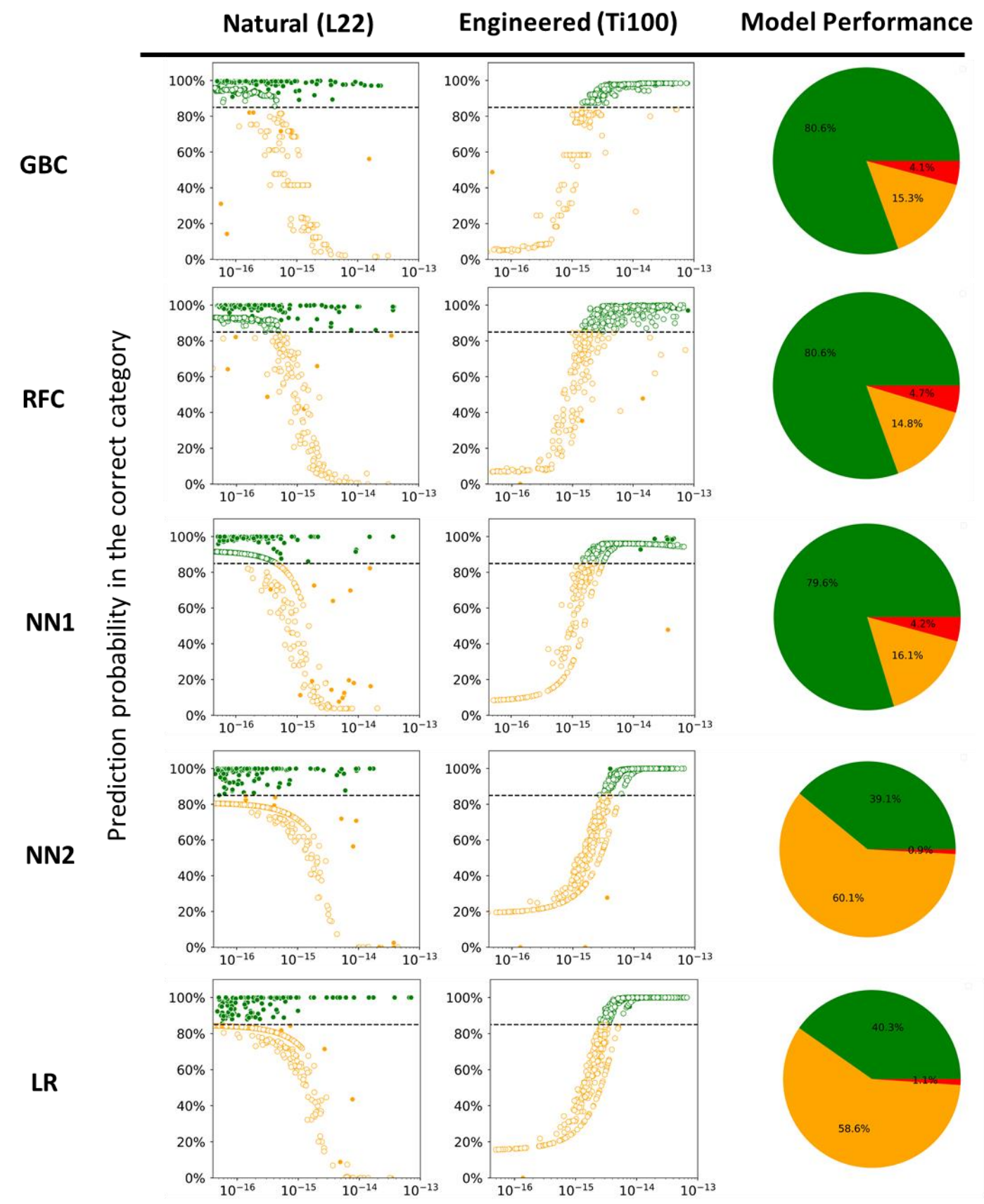
Natural (L22)
Engineered (Ti100)
Model Performance
GBC
RFC
NN1
NN2
LR
Prediction probability in the correct category
Ti Particle Mass (g)
80.6%
4.1%
15.3%
80.6%
4.7%
14.8%
79.6%
4.2%
16.1%
39.1%
0.9%
60.1%
40.3%
1.1%
58.6%

Figure S5: ML results for GBC, RFC, NN1, and NN2 models for the L22 + Ti100 case. Left scatter plots are Ti-NNMs displayed as the probability of the ML predicting in the correct category as a function of Ti mass. Right scatter plots are the same but for Ti-ENMs. The pie charts display the percentage of total Ti-NMs categorized as correct (green), uncertain (orange), and incorrectly classified (red).

Hyperparameter Tuning

Hyperparameters in the ML model were tuned to provide maximum performance. The two major parameters were the inverse of the regularization strength (C) in the LR model and the number of components for NMF. The values of the inverse of regularization strength ranged from 0.001 to 10,000. The performance was measured by testing accuracy for the L22 + Ti100 case. Figure below shows the results for C. The maximum accuracy plateaued at 1,000 so this is the chosen value for C. For the number of components, the values ranged from 5 to 20 components. We found that at 10 components and higher, the testing accuracy did not significantly change, so we chose 10 components for the ML model.

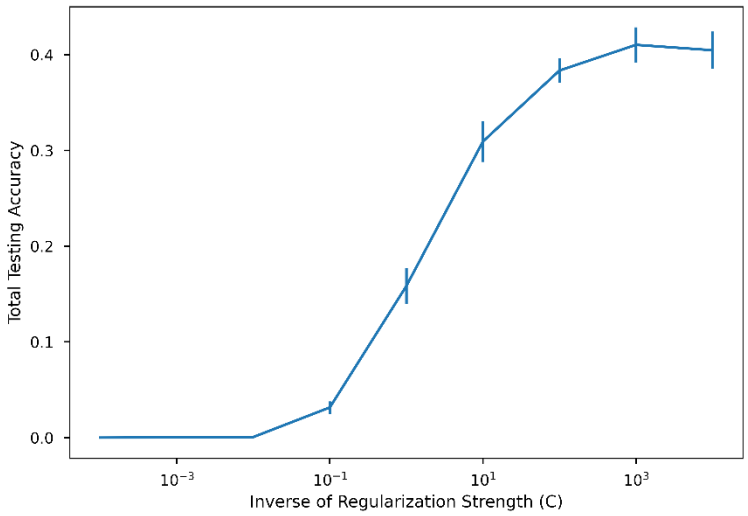

Figure S6: Testing Accuracy for the L22 + Ti100 case as a function of the inverse of the Regularization Strength (C) (number of simulations = 5).

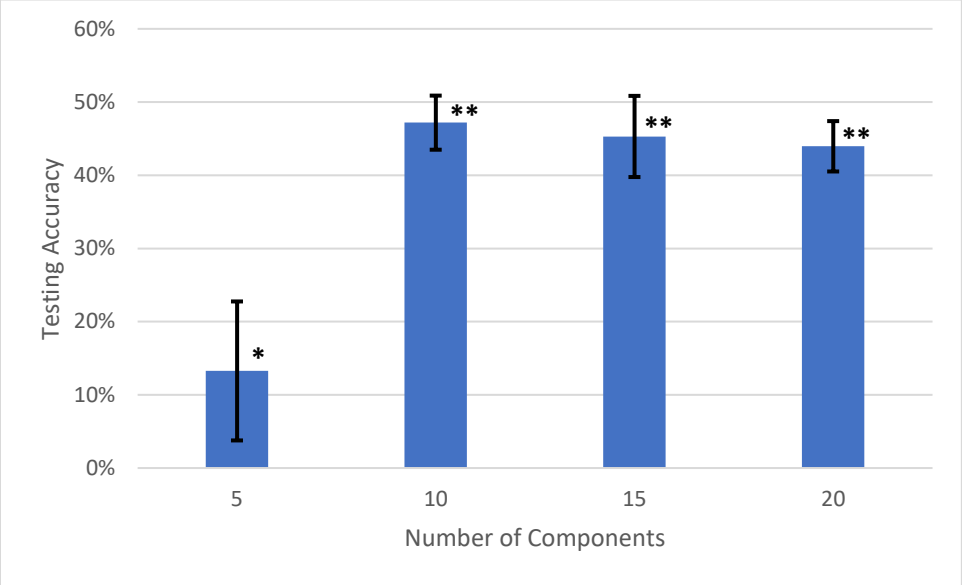

Figure S7: Testing Accuracy for the L22 + Ti100 case as a function of number components for NMF (number of simulations = 5). Symbols represent statistical similarities (One Way ANOVA with P-value > 10^{-2})

Bootstrapping Method to Evaluate Sample Size

To ensure that the training and testing size for each case was sufficient, the bootstrapping method was implemented. This method trains on parts of the training dataset (from 5 to 100%) and plots the accuracy of the model (test data points with > 85% confidence). The random sampling of different parts of the training data is performed five times for each fraction. The whole bootstrapping process is performed three times for each case. Because the particle count and fingerprint are similar between the three soils, we tested three cases: L22 + Ti100, L22 + Ti30, and L22 + Ti-Sludge (Figure S9).

All cases exhibited high variability in the accuracy for each case from 5 for 40%. Starting at 40% or higher, the performance of the model becomes constant. There is slight discrepancy in accuracy for the triplicate simulations of L22 + Sludge and L22 + Ti30 cases but only by 2 to 3%. We conclude that the sample size is large enough to train and assess the performance of the model for each case.

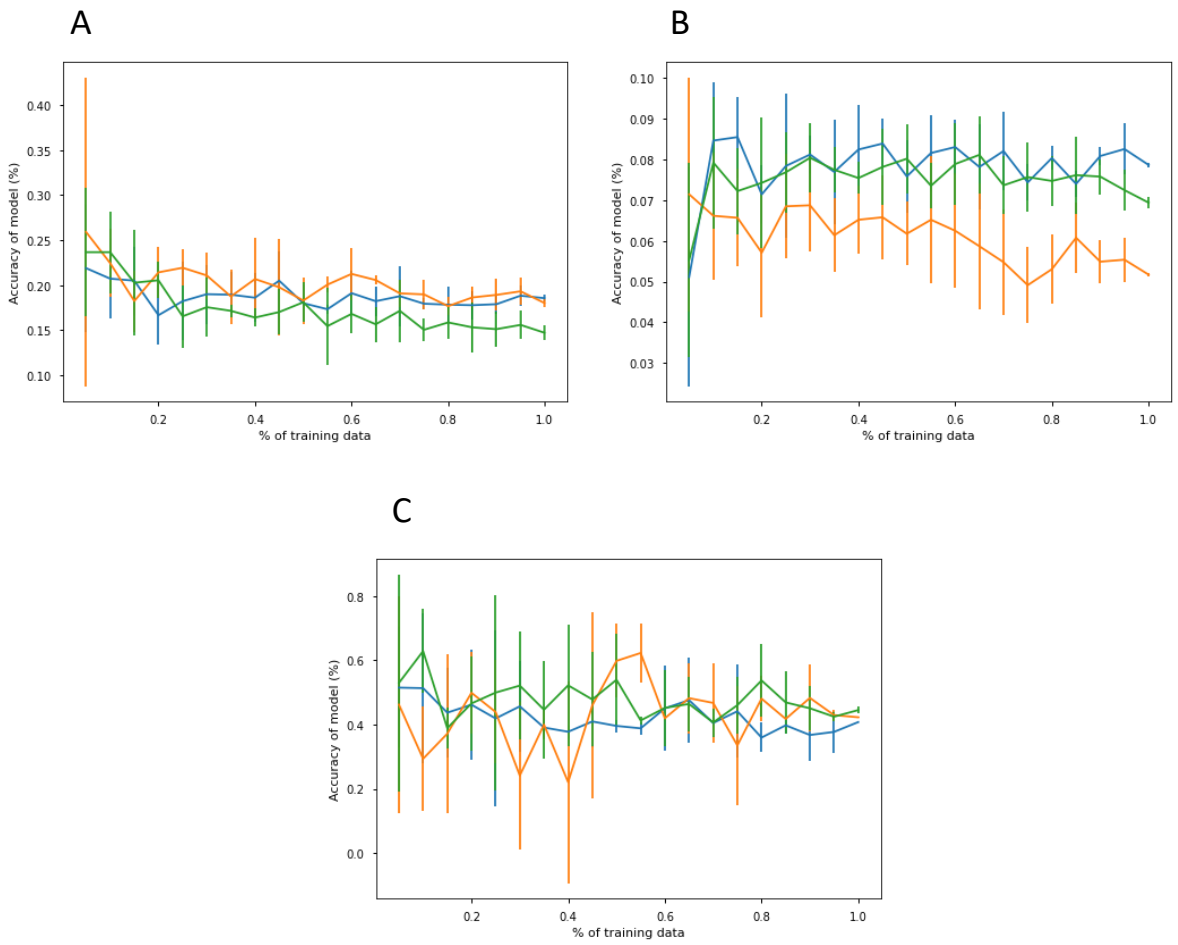

Figure S8: Performance of the model (test data points > 85% confidence) as a function of the percent of the training data for A) L22 + Sludge, B) L22 + Ti30, and C) L22 + Ti100 case.

Isotopes that were tracked with spICP-TOFMS

The following isotopes were tracked for data processing: ^{24}Mg, ^{25}Mg, ^{29}Si, ^{45}Sc, ^{46}Ti, ^{48}Ti, ^{51}V, ^{52}Cr, ^{53}Cr, ^{54}Fe, ^{55}Mn, ^{57}Fe, ^{58}Ni, ^{59}Co, ^{60}Ni, ^{63}Cu, ^{64}Zn, ^{65}Cu, ^{66}Zn, ^{68}Zn, ^{69}Ga, ^{71}Ga, ^{72}Ge, ^{75}As, ^{85}Rb, ^{88}Sr, ^{89}Y, ^{90}Zr, ^{93}Nb, ^{94}Zr, ^{96}Mo, ^{98}Mo, ^{102}Ru, ^{103}Rh, ^{107}Ag, ^{108}Pd, ^{109}Ag, ^{112}Cd, ^{114}Cd, ^{118}Sn, ^{120}Sn, ^{121}Sb, ^{123}Sb, ^{128}Te, ^{130}Te, ^{133}Cs, ^{137}Ba, ^{138}Ba, ^{139}La, ^{140}Ce, ^{141}Pr, ^{142}Ce, ^{144}Nd, ^{151}Eu, ^{152}Sm, ^{153}Eu, ^{154}Sm, ^{156}Gd, ^{158}Gd, ^{159}Tb, ^{162}Dy, ^{164}Dy, ^{165}Ho, ^{166}Er, ^{168}Er, ^{169}Tm, ^{174}Yb, ^{165}Lu, ^{180}Hf, ^{181}Ta, ^{185}Re, ^{190}Os, ^{192}Os, ^{193}Ir, ^{194}Pt, ^{195}Pt, ^{197}Au, ^{200}Hg, ^{202}Hg, ^{206}Pb, ^{208}Pb.

SpICP-TOFMS Parameters

Table S4: spICP-TOFMS Parameters

Plasma Power (W)	1500
Nebulizer Liquid Flow rate (ml/min)	0.35
Nebulizer Gas Flow rate (l/min)	1.02
Attenuated masses (Th)	32, 35, 37, 40
Single Particle Dwell time (ms)	2
Collision gas flow rate (ml/min) *	3 or 0
Transport efficiency	1 – 5%
TOF extraction frequency (extractions per s)	33,000
Nebulizer	Concentric borosilicate glass with 400 µL/min flow rate
Spray Chamber	Baffled cyclonic, high purity quartz
Mass Res Power ^{238}U	> 3000
Auxiliary gas flow rate (L/min)	0.8
Cooling gas flow rate (L/min)	14
TOF Detector type	Microchannel Plate (MCP) Detector

* - Collision gas was used only to test the effect of H_2/He gas mode on Ti and other element detection limits.

More information about the specifics of the spICP-TOFMS 1R system is provided on TOFWerk's website (https://www.tofwerk.com/products/icptof/).

Multi-elemental particle coincidence and polyatomic interference

False positives of multi-elemental particle events can occur by coincidence if two or more separate particles are in the same dwell time interval. To predict this, we used a previously published algorithm to estimate how many coincidental particle events may be present for the three soils and sludge.[4] We then calculated the fraction of particle events that could be coincidental (Table S4).

Common earth-abundant elements like Fe, Mg, Ba, Pb and Mn were predicted to have at least one potential coincidental particle event with Ti, but this is less than 5% of the measured particles containing those elements. Rare earth elements, mostly Ce and La, also had some coincidence (8 to 20% of 10's of particle events). For the Arizona soil, Sc and one isotope of Cr was over 100%, but there were only 1 and 2 particle events respectively. Overall, there is a small fraction of the multielement Ti particle events that could be false positives.

For ^{48}Ti, Ca is the main interference, but we also analyze another more abundant isotope, ^{44}Ca, and did not find any Ca particle events in our samples. We tracked multiple isotopes for most elements to confirm their presence. An example is Sn and Ag particle events in sludge. These particle events were confirmed with two of the main isotopes instead of one (^{107}Ag, ^{109}Ag, ^{118}Sn, ^{120}Sn).

Table S5: The fraction of Ti + another element containing particles that could be coincidental

Isotopes	Lufa 2.2	Arizona	Luvisol	Sludge
24Mg	0.01	0.07	0.01	0.07
25Mg	0.03	0.05	0.03	
45Sc		1.76		
46Ti	0.01	0.02	0.01	
48Ti	0.01	0.02	0.01	
51V	0.02	0.03	0.01	
52Cr	0.90	1.01	0.21	
53Cr			0.04	
54Fe	0.00	0.01	0.00	
55Mn	0.06	0.05	0.05	
57Fe	0.02	0.03	0.01	
58Ni	0.76	0.26	0.05	
59Co	0.06	0.12	0.03	
60Ni		0.14		0.01
63Cu	0.03	0.04	0.04	0.02
64Zn	0.14	0.06	0.03	0.02
65Cu	0.06	0.08	0.02	0.01
66Zn	0.16	0.21		
68Zn	0.21	0.76	0.18	
69Ga	0.11	0.20	0.03	
75As	0.02			
85Rb	0.03	0.04	0.02	
87Rb	0.04	0.06	0.01	
88Sr	0.09	0.27	0.04	0.01
89Y	0.08	0.13	0.05	
90Zr	0.05	0.07	0.04	0.01
93Nb	0.01	0.02	0.01	
94Zr	0.09	0.10	0.11	0.01
96Mo	0.05	0.12		
98Mo			0.01	

Isotopes	Lufa 2.2	Arizona	Luvisol	Sludge
107Ag				0.02
109Ag		0.05		0.06
118Sn		0.04		
123Sb	0.04			
128Te		0.12		
133Cs	0.02	0.07	0.01	
137Ba	0.03	0.08	0.02	
138Ba	0.04	0.10	0.03	
139La	0.17	0.20	0.10	
140Ce	0.10	0.09	0.08	
141Pr	0.10	0.18	0.04	
142Ce	0.08	0.18	0.09	
142Nd	0.08	0.18	0.09	
144Nd	0.10	0.11	0.13	
152Sm		0.05		
153Eu	0.02			
154Sm		0.14		
156Gd		0.27		
158Gd		0.16		
164Dy	0.02	0.09		
165Ho	0.02	0.14		
166Er		0.11		
168Er		0.11		
181Ta	0.01	0.08		
200Hg				
202Hg				
206Pb	0.02	0.04	0.01	
208Pb	0.02	0.04	0.01	
238U		0.08	0.01	

Mass Distribution of Ti-NMs

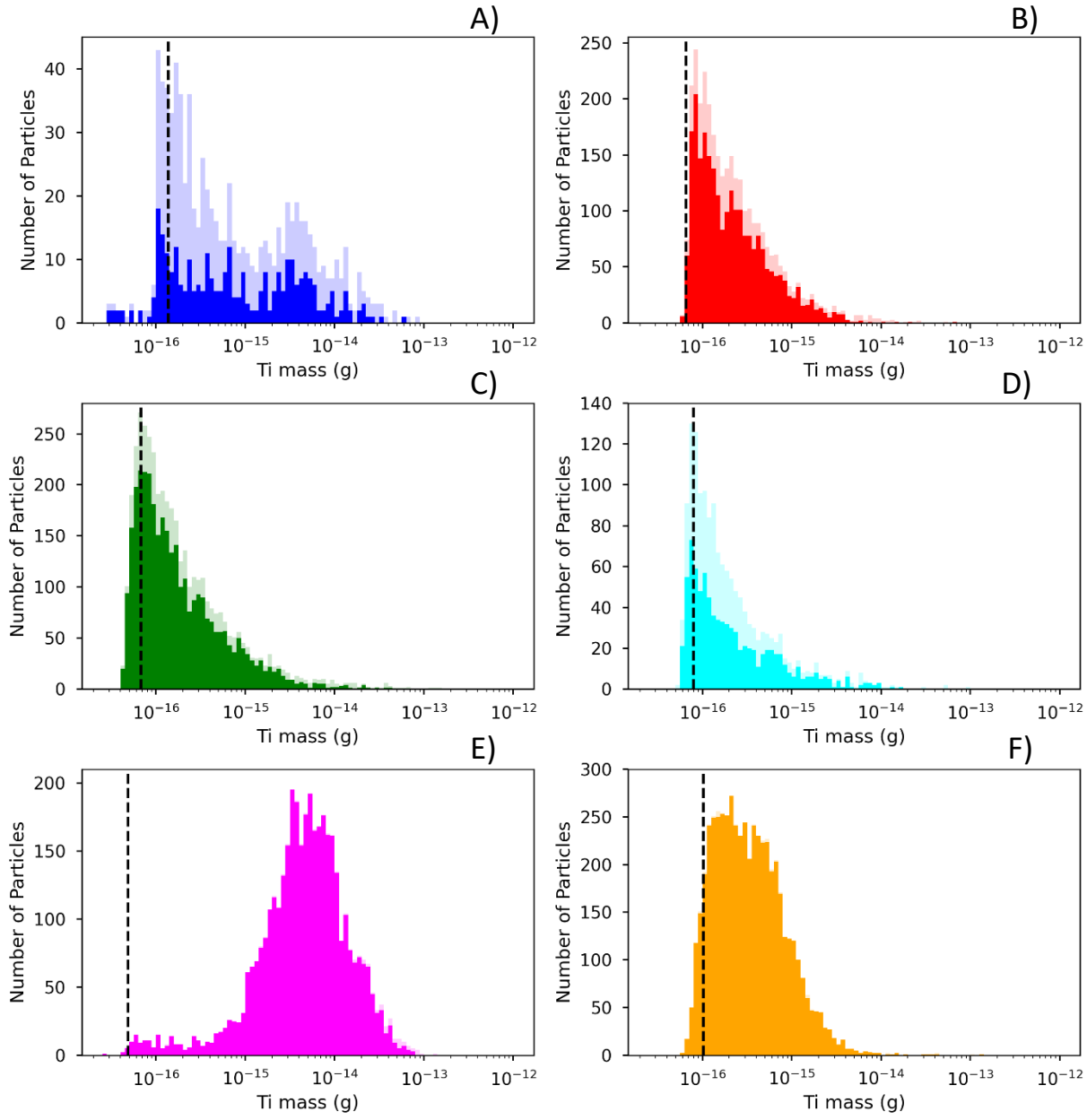

Figure S9: Ti particle mass distribution (as measured by ^{48}Ti) for each sample (A: Sludge, B: ARZ, C: L22, D: LUV, E: Ti100, F: Ti30). Faded color histogram represent total Ti particle and the filled color histogram is pure Ti particles (i.e., Ti-particles not associated with other elements). Black dashed line indicates the average IUPAC threshold extracted from background signal files for each sample.

Remaining Test Cases of the ML Simulations

The remaining cases for classification by the ML model are shown in the figure below. The Ti30 + ARZ and Ti30 + LUV have a similar performance compared to the Ti30 + L22 case with a portion of NNM being correctly classified regardless of Ti-mass (NNMs with elemental associations). The NNMs without elemental associations were categorized as uncertain because of the similar mass distribution with Ti30 ENMs. Similar to Ti30 + L22 case, most ENMs were categorized as uncertain. For the recovered Ti-NMs from sludge, the model also had a similar performance compared to the Ti-NMs from sludge + L22 case. Elemental association in the recovered Ti-NMs were primarily used while most of the NNMs were categorized as uncertain. There are a few ARZ and LUV NNMs that were correctly classified which most likely had unique tracers. For both cases, the recovered Ti-NMs without elemental associations followed a sigmoidal curve with increasing confidence of being in the correct category as Ti-mass increases.

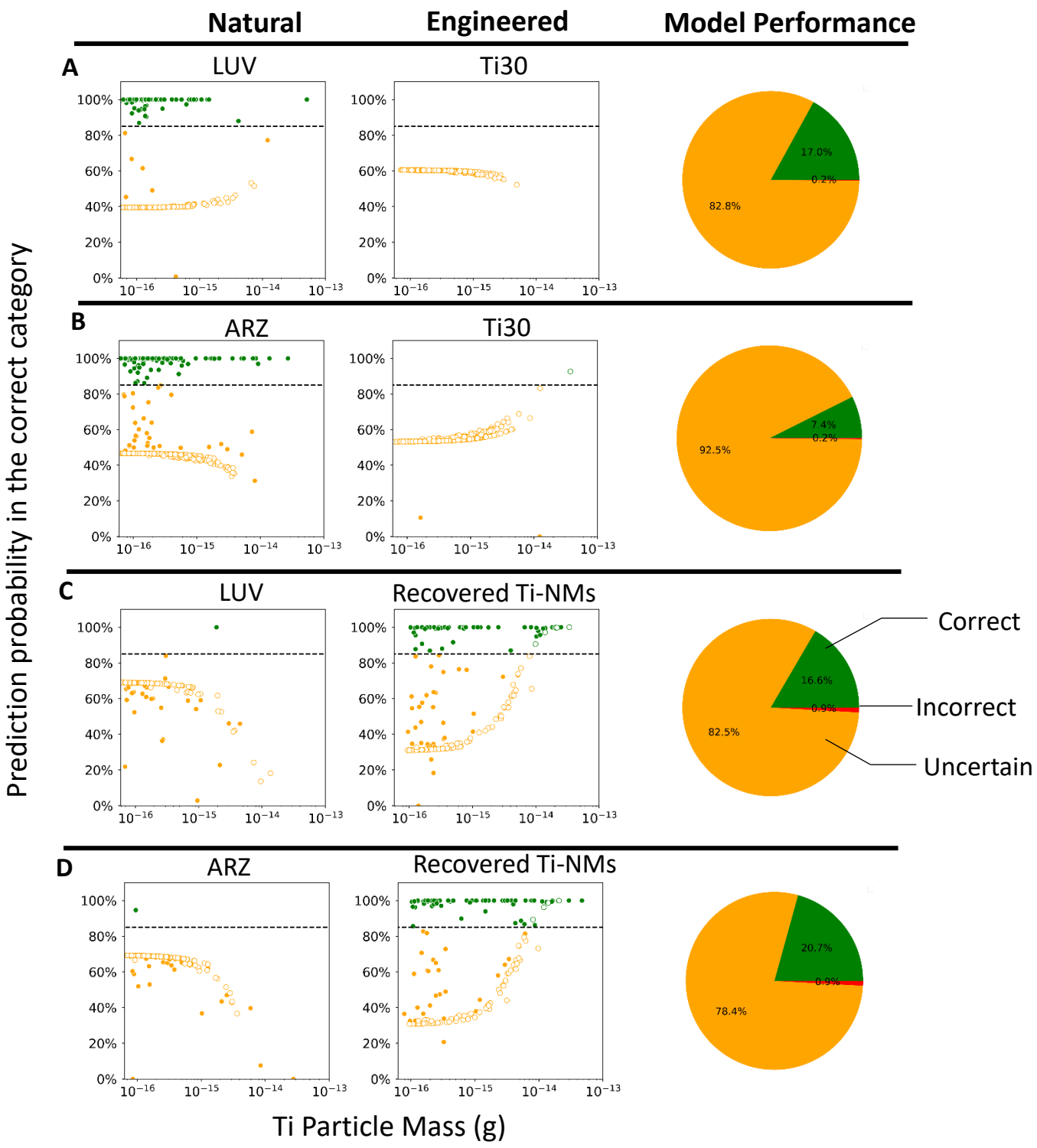

Figure S10: ML results of the testing data for each test case (LUV + Ti30, ARZ + Ti30, LUV + Sludge, ARZ + Sludge). Left scatter plots are Ti-NNMs displayed as the probability of the ML

predicting in the correct category as a function of Ti mass. Right scatter plots are the same but for Ti-ENMs. The pie charts display the percentage of total Ti-NMs categorized as correct (green), uncertain (orange), and incorrectly classified (red).

Elemental Fingerprint for each Test Case

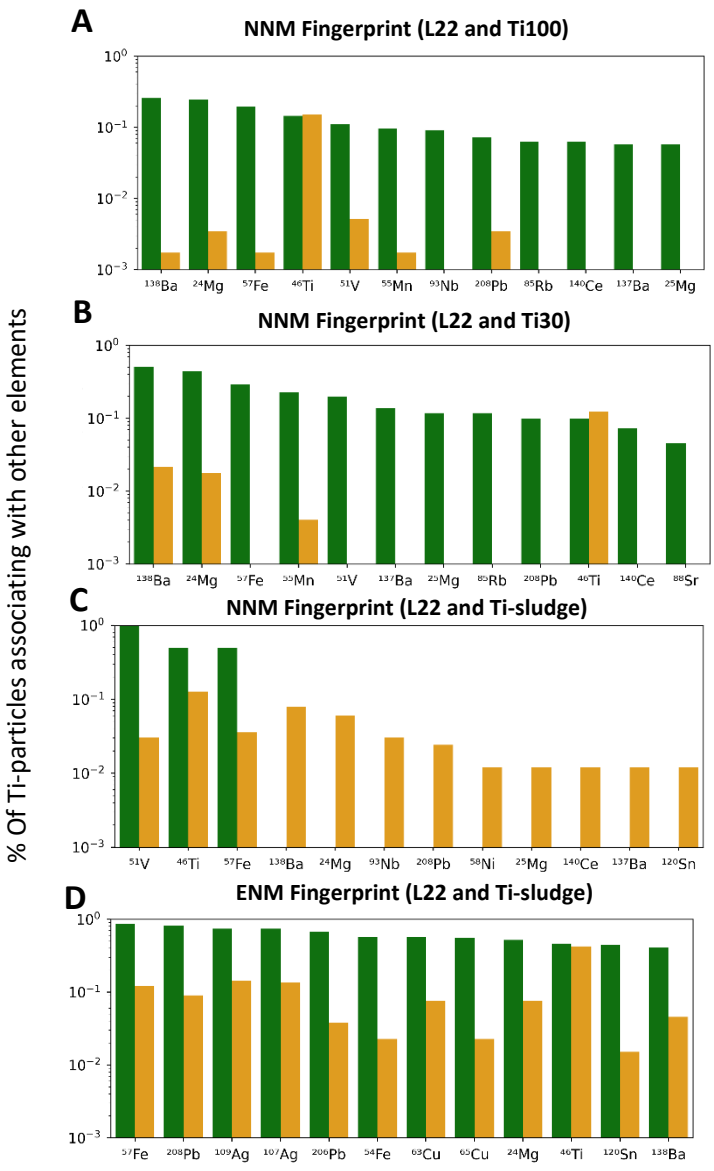

Figure S11: Elemental associations with Ti-particles increases the probability of predicting it in the correct category. The elemental fingerprint was measured for A) L22 Ti-NNMs from L22 + Ti100 case, B) L22 Ti-NNMs from L22 + Ti30 case, C) L22 Ti-NNMs from L22 + Ti-sludge case, and D) Ti-ENMs from L22 + Ti-sludge case. Green represent Ti-NMs correctly classified (> 85%) and orange is uncertain or misclassified (<85%). ^{46}Ti is represented in here as a minor element

associated with ^{48}Ti particle events. In Figure 2, the open circles represent ^{48}Ti and ^{48}Ti + ^{46}Ti particle events.

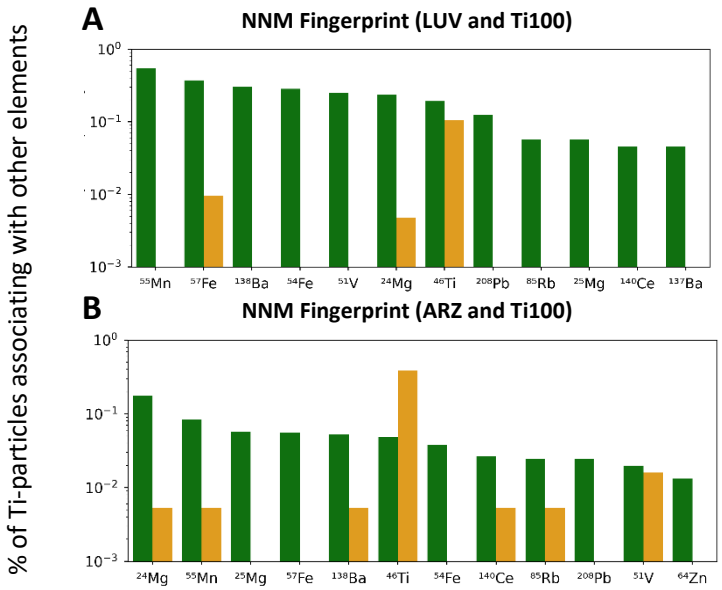

Figure S12: The elemental fingerprint for A) LUV Ti-NNMs from LUV + Ti100 and B) ARZ Ti-NNMs from ARZ + Ti100. Green represent Ti-NMs correctly classified (> 85%) and orange is uncertain or misclassified (<85%). Bar plots indicate the most common isotope associations with Ti NMs showing the drastic differences in abundance of elemental fingerprints between correctly classified and uncertain.

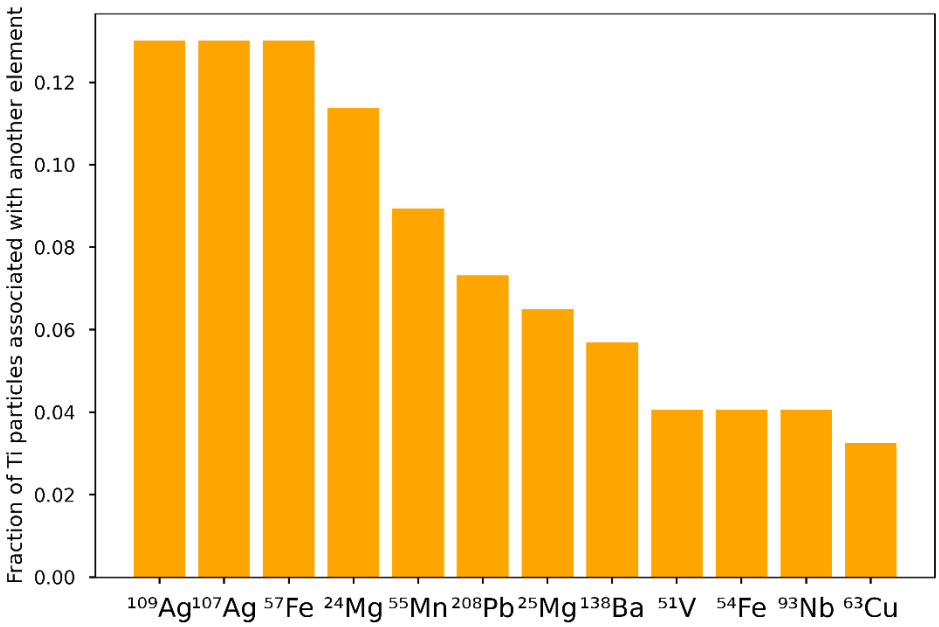

Figure S13: The fraction of Sludge-Ti NMs in the 'uncertain' category associated with other elements for the L22 + Sludge case. All elements are common with L22 soil particle except for Ag. Even though Ag is the most attached element in the uncertain category, most of the Ti + Ag contained particles (80%) were confidently classified. If hard classification was applied (e.g., confidence greater than 50%), then all Ag + Ti would predict correctly.

Element Importance for each Test Case

For each test case, the elemental importance was calculated according to the equation below.

$$Magnitude = P_{occurence} \left| \sum_{i=1}^{10} C_i C_{element,i} \right|$$

Where $P_{occurence}$ is the probability of the occurrence of a particle event for a given element in a sample, C_i is the NMF component coefficient, and $C_{element,i}$ is the coefficient for a given element within a component. For binomial logistic regression, component coefficients are negative for "Engineered" label and positive for "Natural" label. For clarification in the figures,

the absolute value of the sum component is used and labeled “Engineered” with blue and “Natural” with red.

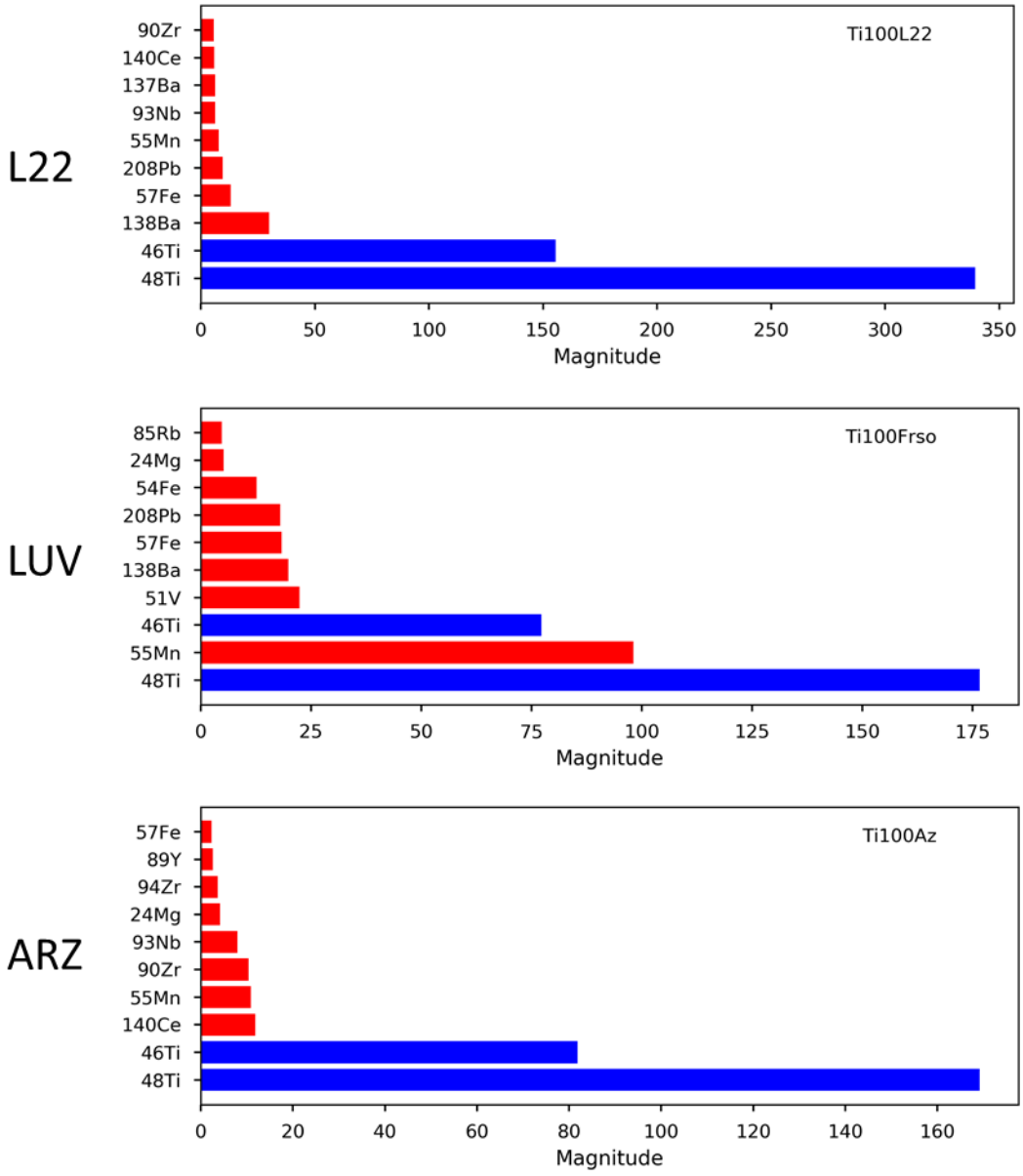

Figure S14: Magnitude of the top 10 elements for L22, LUV, ARZ and Ti100 cases. Blue bars represent the “Engineered” label and red represent “Natural”.

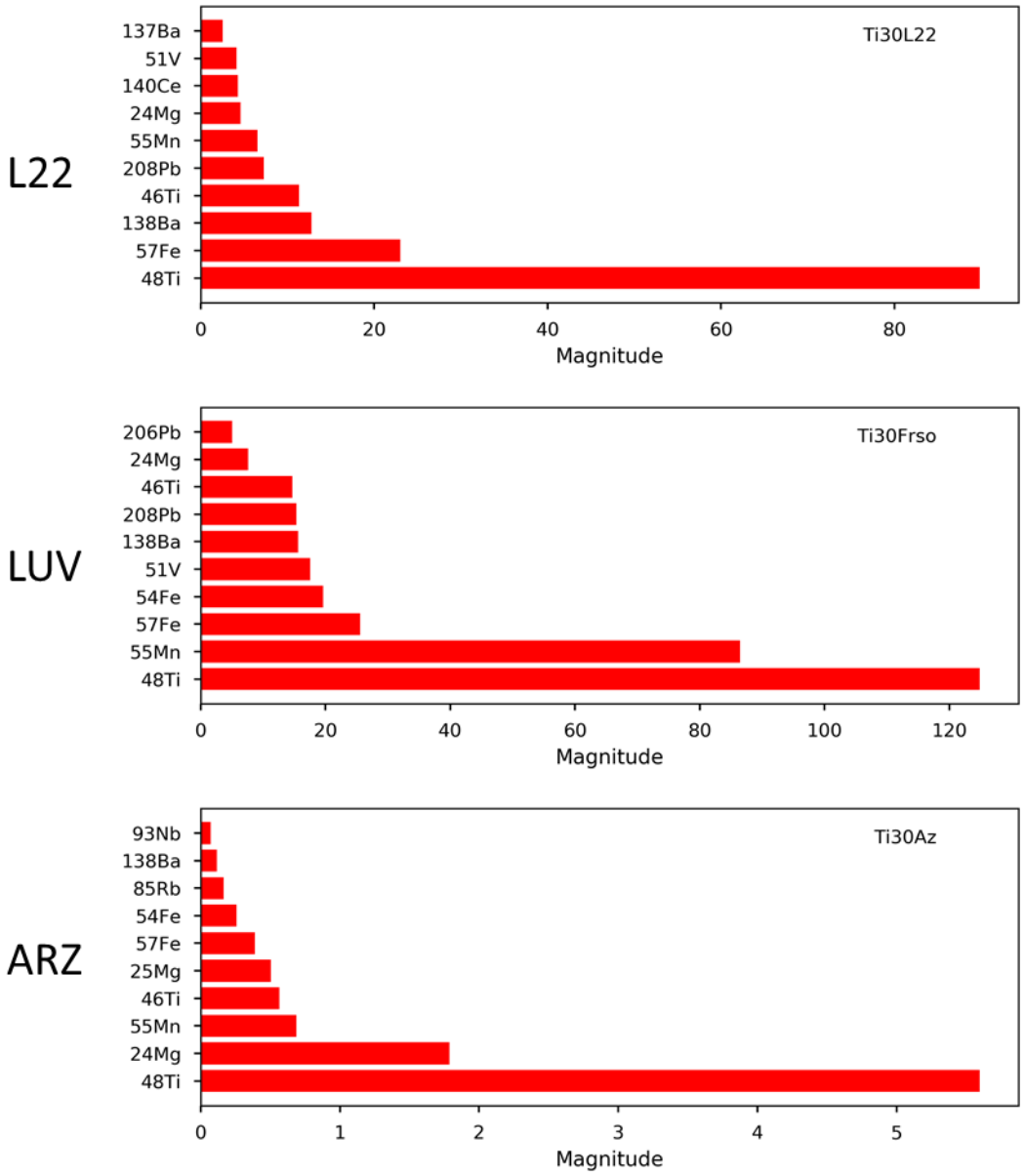

Figure S15: Magnitude of the top 10 elements for L22, LUV, ARZ and Ti30 cases. Blue bars represent the "Engineered" label and red represent "Natural".

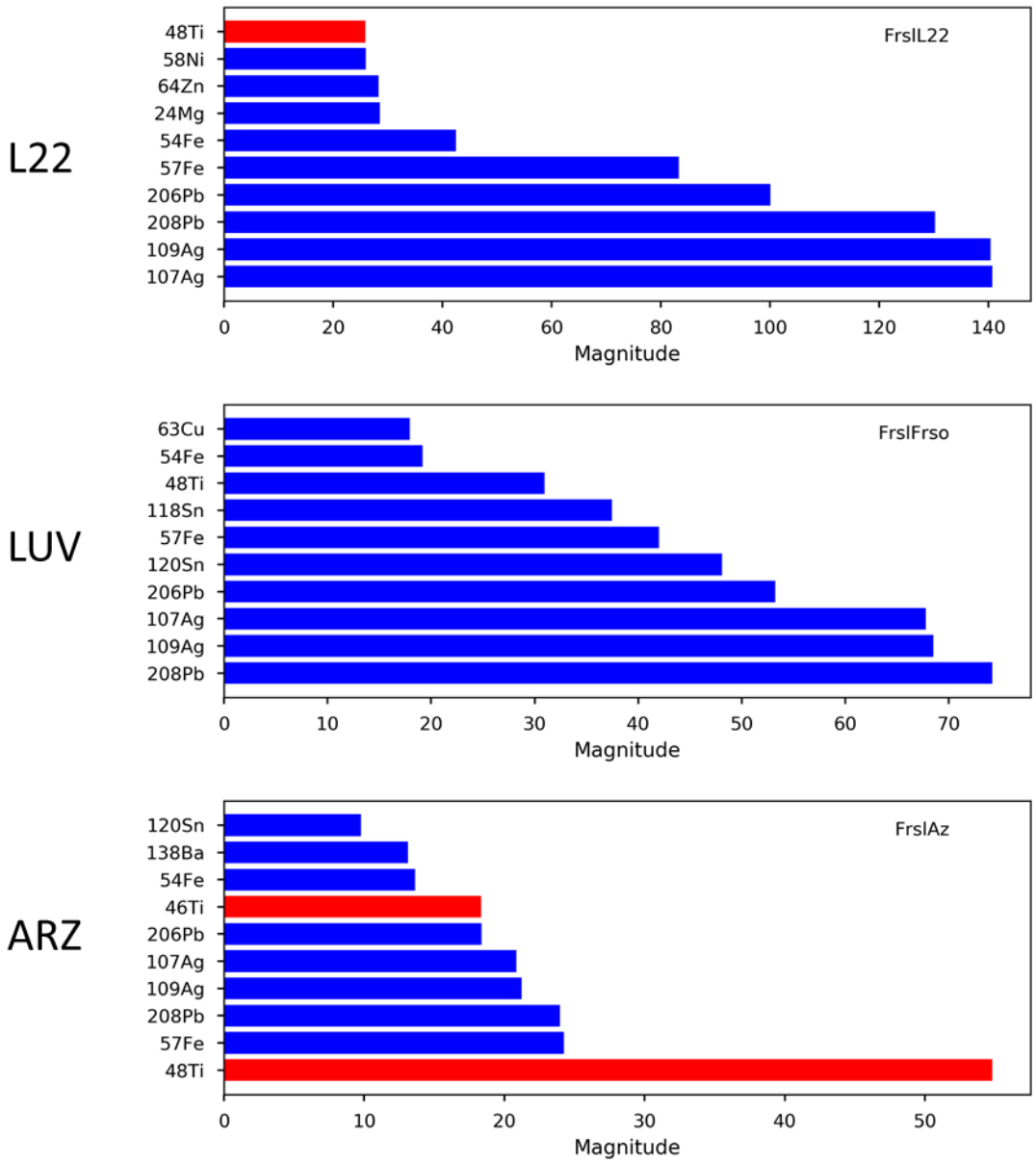

Figure S16: Magnitude of the top 10 elements for L22, LUV, ARZ and Recovered Ti-NMs in sludge cases. Blue bars represent the "Engineered" label and red represents "Natural".

The effect of H_2/He mode measurement by spICP-TOFMS

Adding a collision cell gas reduces isobaric interferences for specific analytes which can influence analyte sensitivity. To determine if this improved the classification of ENMs and NNMs, L22 and Ti100 samples were measured by spICP-TOFMS with a H2/He collision cell gas (2% H_2 /98% He). The ML model was then trained and tested with these samples to determine classification results and elemental importance (Figure S11 and S12). Classification did not improve when including a H_2/He collision cell gas. The LR model correctly classified 27% of the Ti-particles and the remaining were uncertain or misclassified. This increased misclassification is due to a few reasons. First, the size distribution difference between L22 and Ti100 is significantly smaller than in normal mode (L22 is 113 ± 51 nm and Ti100 is 189 ± 65 nm). This change is due to decreased sensitivity of Ti^{48}, therefore an increase in detection limit. Second is the overall decrease sensitivity of other important analytes (Nb, Mn, Ba, Mg, Rare Earth Elements). However, Si^{28} and Fe^{56} sensitivity greatly increases because of eliminating Ar gas interferences and has a much higher importance within the model (Figure S5). For Ti classification, we do not recommend measuring particles with a H_2/He collision gas.

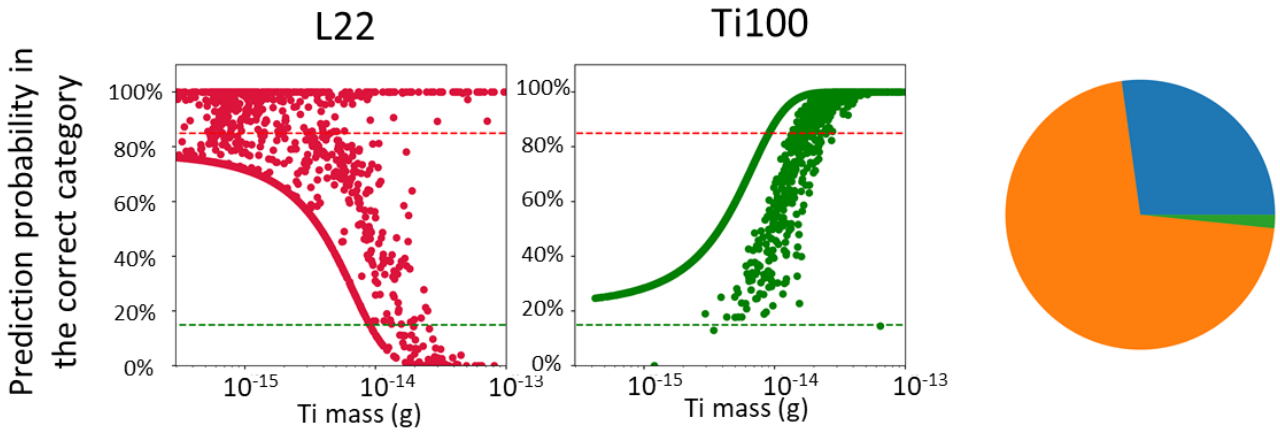

Figure S17: LR model prediction of Ti-particles as a function of ENM (right) and NNM (left) and Ti-mass for Ti100 and L22 case measured by spICP-TOFMS with H_2/He collision cell gas.

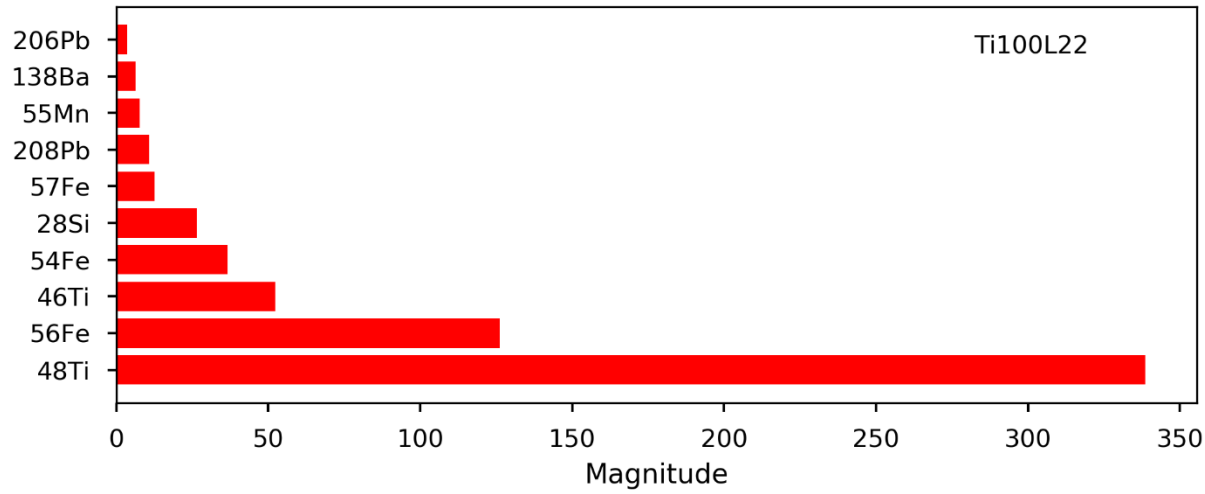

Figure S18: Magnitude of the top 10 elements for L22 and Ti100 case measure by spICP-TOFMS with H_2/He collision cell gas.

Investigating the effect of Al in Ti classification

Ti can associate with Al either by Ti substitution in clay particles or a Ti-particle associating with clay particles. Because of these associations, impure Ti particles in the natural category may associate elements that are inherently not present as unique tracers for Ti minerals. We investigate the effect of Al associating with Ti for the L22 soil and how that impacts classification for the Ti100 ENMs. For the L22 soil, 33% of Ti particles is associated with Al. First, we determined if natural Ti-particles in L22 are substituted clay particles. In kaolin and bentonite, the substituted Ti can range from 0.01 to 2.12% by mass which means the Ti to Al ratio in these minerals can be up to 10.4% .[5,6] For the Ti + Al particle in L22, the median is 7.94% and most of these particles are within the typical range for Ti-substituted particles. This shows that a significant amount of natural Ti + Al particles could be Ti substituted particles.

For this study, we will assume all Ti + Al particles are Ti substituted clay particles. We excluded all Ti + Al (+ any other element) particles from the natural category and tested this for classification with the Ti100 particles (Figure S13). The classification performance slightly decreased (35% correctly classified), but overall preserved the same trends. Rather than using common earth-abundant elements (Ce, Mg, Ba, etc.) from the first scenario, Nb, V, and Mn are the top weighted elements which are likely impurities in Ti minerals. This concludes that the model's performance is not affected by Ti's association with Al (and other elements) that may be a Ti substituted clay particle or a pure Ti particle attached to a clay mineral.

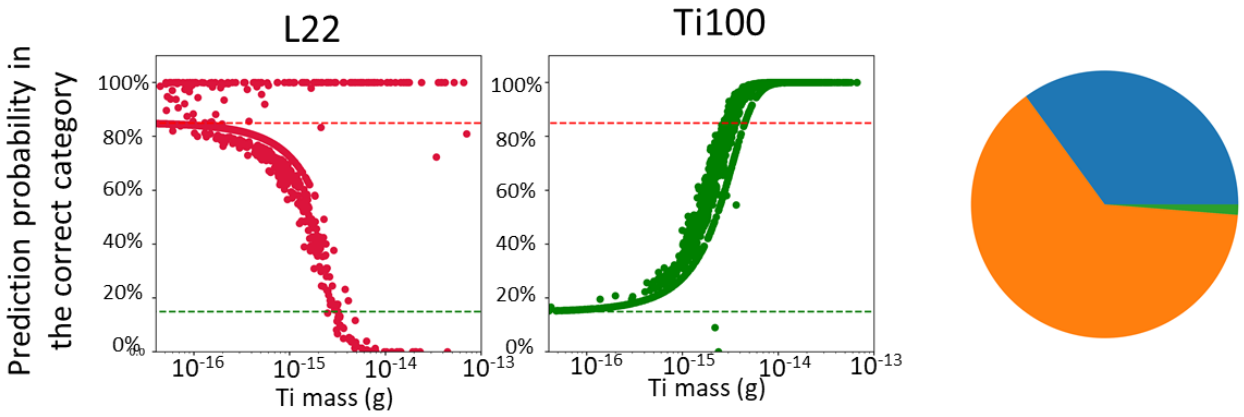

Figure S19: ML model prediction of Ti-particles as a function of ENM (right) and NNM (left) and Ti-mass for Ti100 and L22 case excluding Ti particles associated with Al. Pie chart to the right shows the model performance predicting correctly (blue, ≥85%), uncertain (orange, 15% ≤ particles < 85%), or misclassified (green, < 15%).

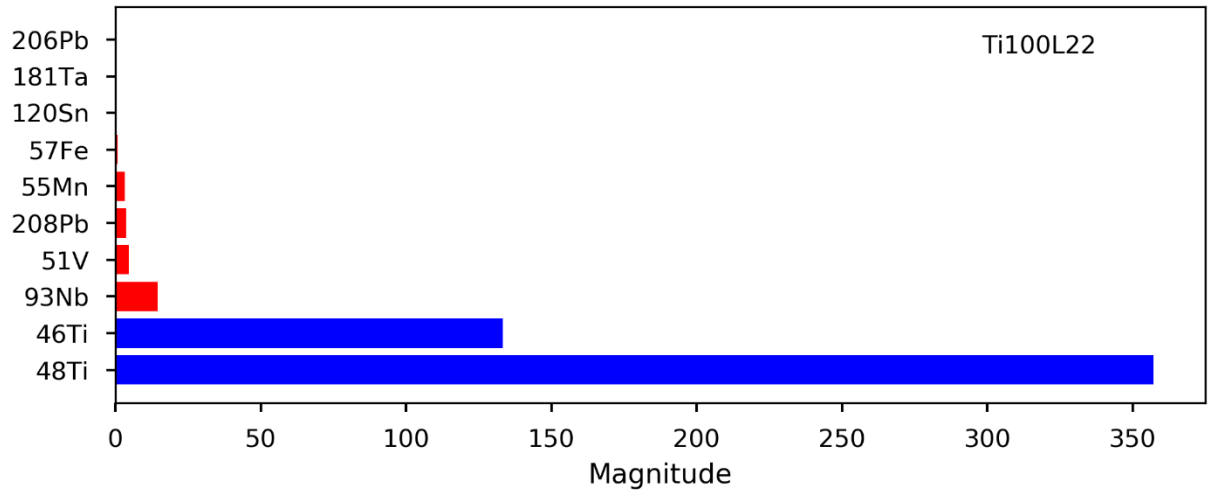

Figure S20: Magnitude of the top 10 elements for L22 and Ti100 case measured by spICP-TOFMS excluding Ti particles associated with Al.

The effect of pretreating Ti30 sample on classification

The high level of uncertainty for the Ti30 + NNM scenarios could be caused by outliers in the Ti30 particles. One way to mitigate this issue is to eliminate all elemental information in the Ti30 sample. We investigated the effect of pretreating the Ti30 sample by removing all other elemental associations on classification, specifically for the L22 + Ti30 test case. There is a slight improvement compared to not pretreating Ti30 with more particles predicted as the correct category. There is also a greater distinction between pure and impure Ti-particles. However, the improvement is negligible with <10% particles being correctly classified. Therefore, this strategy was not implemented for the remaining test cases.

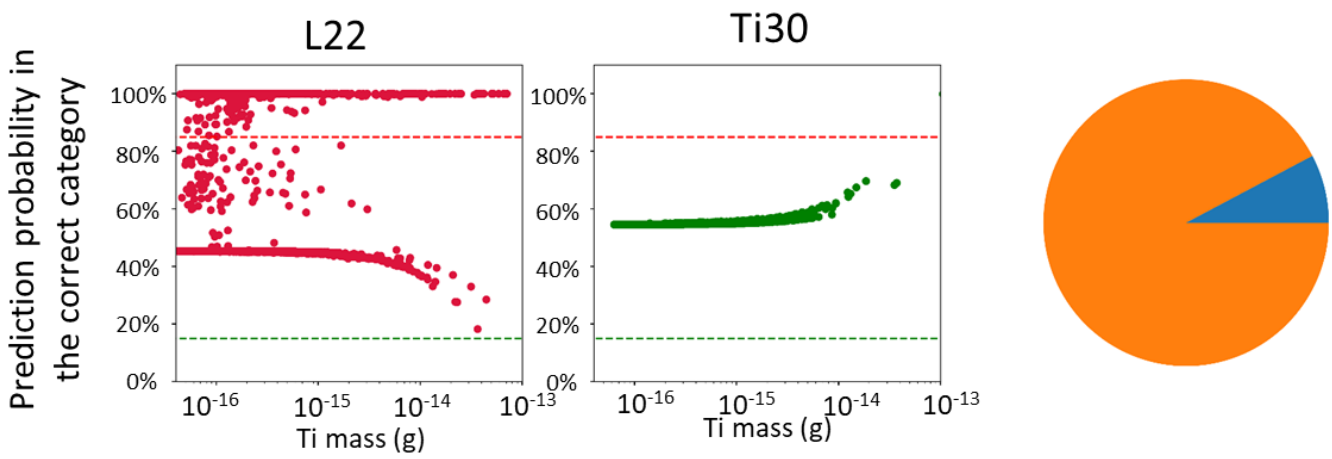

Figure S21: LR model prediction of Ti-particles as a function of ENM (right) and NNM (left) and Ti-mass for Ti30 and L22 case including a pretreatment of Ti30 sample. Pie chart to the right shows the model performance in either predicting correct (blue, ≥85%), uncertain (orange, 15% ≤ particles < 85%), or misclassified (green, < 15%).

Ti Concentrations measured by ICP-OES

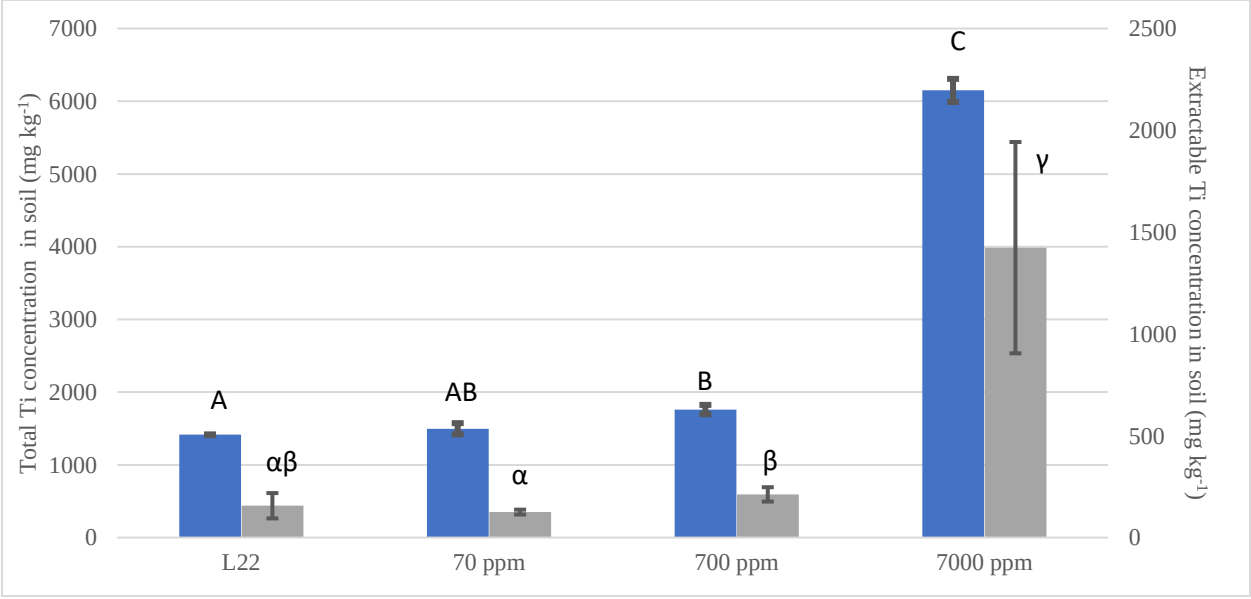

Figure S22: Ti concentration of L22 soils dosed at 0, 70, 700, and 7,000 mg kg^{-1} of TiO_2 measured by ICP-OES. Blue bar is the total Ti concentration in the soil (n =2). Gray bar is the extractable <500nm Ti concentration (n = 3). Letters and symbols represent statistical similarities for one-way ANOVA (P value < 0.02) comparing each trial's total soil Ti concentration and extractable Ti concentration (mg-Ti kg^{-1}-soil).

References

(1) Pradas del Real, A. E.; Castillo-Michel, H.; Kaegi, R.; Larue, C.; de Nolf, W.; Reyes-Herrera, J.; Tucoulou, R.; Findling, N.; Salas-Colera, E.; Sarret, G. Searching for Relevant Criteria to Distinguish Natural *vs.* Anthropogenic TiO $_2$ Nanoparticles in Soils. *Environ. Sci. Nano* **2018**, 2853–2863. https://doi.org/10.1039/C8EN00386F.

(2) Gao, X.; Rodrigues, S. M.; Spielman-Sun, E.; Lopes, S.; Rodrigues, S.; Zhang, Y.; Avellan, A.; Duarte, R. M. B. O.; Duarte, A.; Casman, E. A.; Lowry, G. V. Effect of Soil Organic Matter, Soil PH, and Moisture Content on Solubility and Dissolution Rate of CuO NPs in Soil. *Environ. Sci. Technol.* **2019**, *53* (9), 4959–4967. https://doi.org/10.1021/acs.est.8b07243.

(3) Simonin, M.; Guyonnet, J. P.; Martins, J. M. F.; Ginot, M.; Richaume, A. Influence of Soil Properties on the Toxicity of TiO2 Nanoparticles on Carbon Mineralization and Bacterial Abundance. *J. Hazard. Mater.* **2015**, *283*, 529–535. https://doi.org/10.1016/j.jhazmat.2014.10.004.

(4) Mehrabi, K.; Kaegi, R.; Günther, D.; Gundlach-Graham, A. Emerging Investigator Series: Automated Single-Nanoparticle Quantification and Classification: A Holistic Study of Particles into and out of Wastewater Treatment Plants in Switzerland. *Environ. Sci. Nano* **2021**. https://doi.org/10.1039/d0en01066a.

(5) Dolcater, D. L.; Syers, J. K.; Jackson, M. L. Titanium as Free Oxide and Substituted Forms in

Kaolinites and Other Soil Minerals. *Clays Clay Miner.* **1970**, *18* (2), 71–79. https://doi.org/10.1346/CCMN.1970.0180202.

(6) Malengreau, N.; Muller, J. P.; Calas, G. Spectroscopic Approach for Investigating the Status and Mobility of Ti in Kaolinitic Materials. *Clays Clay Miner.* **1995**, *43* (5), 615–621. https://doi.org/10.1346/CCMN.1995.0430511.